Faraday Discussions
Cite this: *Faraday Discuss.*, 2026, **263**, 123

PAPER

Supramolecular interactions in softwood kraft lignin nanoparticles†

Massimo Sgarzi, *[a] Matteo Gigli, [a] Shahzal Babar,[a] Nicolò Pajer, [a] Giorgia Peroni,[a] Claudia Crestini, *[a] Nina Tverdokhleb, [b] Arezoo Dianat, [b] Rafael Gutierrez [b] and Gianaurelio Cuniberti [bc]

Received 10th May 2025, Accepted 26th June 2025
DOI: 10.1039/d5fd00076a

The production of functional (nano)materials based on lignin as a renewable starting material depends on the thorough understanding of lignin's physico-chemical properties, among which self-assembly and agglomeration/aggregation are the most important. Nevertheless, the knowledge about the structure–property relations for lignin is still in its infancy and needs further in-depth investigations. In this context, this works focuses on the study of the size and the colloidal stability of lignin nanoparticles (LNPs) prepared from softwood kraft lignin (SKL) using the solvent–antisolvent method. Conformational rearrangements of lignin chains were found to contribute significantly to the formation of the first lignin nuclei. The slow addition of ethylene glycol and THF into water caused the formation of nuclei with low aggregation numbers, minimizing the hydrodynamic volume of the final LNPs. On the other hand, a quick addition of these organic solvents created spatially and temporally higher lignin concentrations, yielding nuclei with high aggregation numbers and larger hydrodynamic volumes. Molecular dynamics simulations revealed the major role of intramolecular and intermolecular hydrogen bonds in this process, together with the contribution from π–π stacking interactions. The superficial concentration of phenolic and condensed guaiacyl units was found to strongly influence the corresponding LNPs' zeta-potential values. Altogether, these results shed further light on the properties of colloidal lignin with a view to enabling its full potential as a key material for technological applications.

1 Introduction

Technical lignins are obtained as byproducts of pulp and paper and modern biorefinery processes and represent the most abundant low-cost aromatic

[a]*Department of Molecular Sciences and Nanosystems, Ca' Foscari University of Venice, Via Torino 155, 30172 Venice, Italy. E-mail: massimo.sgarzi@unive.it; claudia.crestini@unive.it*
[b]*Institute for Materials Science and Max Bergmann Center for Biomaterials, TUD Dresden University of Technology, 01062, Dresden, Germany*
[c]*Dresden Center for Computational Materials Science (DCMS), TUD Dresden University of Technology, 01062 Dresden, Germany*

† Electronic supplementary information (ESI) available. See DOI: **https://doi.org/10.1039/d5fd00076a**

biopolymer, with a yearly production reaching 100 million tons.[1] The polyphenolic structure that characterizes these biopolymers endows them with antioxidant and antibacterial properties, together with UV-shielding properties,[2–4] and makes them potential candidates to substitute oil-based chemicals.[5]

Nevertheless, the valorisation of lignin remains a very challenging task for several reasons. The first is the structural heterogeneity of this biopolymer, whose biosynthesis proceeds *via* oxidative enzymatic radical reactions of *p*-coumaryl, coniferyl and sinapyl alcohols to yield polydisperse phenylpropanoid oligomers lacking a regular pattern of repeating units, with a random distribution of linkage motifs.[6,7] The second is that its composition depends on the plant species:[8,9] lignin originating from gymnosperms is typically constituted by guaiacyl units, while dicotyledonous angiosperms additionally contain syringyl units; monocotyledons are composed of guaiacyl, syringyl and *p*-hydroxyphenyl units. The third is the structural modifications that lignin undergoes during the numerous processes utilized for its isolation, which can subsequently drastically modify its physico-chemical properties.[6,8,10] The fourth, but not least, is its poor solubility in most of the commonly used solvents.[11]

As a result, only 2% of the total amount of lignin produced every year is utilized for the production of value-added chemicals and materials, while 98% of it is incinerated as heating fuel.[12]

Despite this complex scenario, thanks to the self-assembly ability of lignin molecules,[13–15] an ever-growing pathway of lignin valorisation is the preparation of nanomaterials (nanoparticles, nanocapsules and nanocomposites), whose application fields span from agriculture, through the food industry, to biomedicine.[16–20]

The full exploitation of lignin as a renewable starting material for the production of functional nanomaterials and especially nanoparticles depends on the thorough understanding of its physico-chemical properties. Nevertheless, a clear rationalization of the structure–property relations of lignin is still in its infancy.[14,15,21,22]

The self-assembly properties of lignin can be described in terms of DLVO theory, through a combination of long-range (*e.g.*, van der Waals, electrostatic and hydrophobic) and short-range (*e.g.*, hydrogen bonding and π–π stacking) interactions, which originate from the inherent structural heterogeneity of lignin.[15,23] An important contribution in self-assembly is expected to arise from the interface between lignin and its microenvironment, where the arrangement of the exposed functional groups of lignin is of utmost importance. Moreover, when nanoparticles are considered, the presence of acid–base active functional groups in lignin (such as carboxylic and phenolic groups) is anticipated to govern the colloidal stability of the species.

In addition, the relative contribution of long-range and short-range interactions driving the formation of lignin nanoparticles (LNPs) is determined by the preparation methodology.[24] The most extensively investigated methods are pH shifting (also known as acid precipitation) and solvent–antisolvent (also known as solvent shifting or nanoprecipitation) approaches. The former involves the dissolution of lignin at alkaline pH (>10) and the subsequent acidification to acidic pH (<5).[25] Conversely, the solvent–antisolvent approach first dissolves lignin into organic solvents, which can be mixed with water (*e.g.*, acetone, ethanol, DMSO and THF). The obtained lignin solution is subsequently

added to an excess amount of the antisolvent water, resulting in the formation of LNPs.[26]

The pH-shifting method typically allows obtaining smaller nanoparticles (<100 nm) with more compact cores, while the solvent–antisolvent method yields larger nanoparticles (>100 nm) with less dense cores.[27] Moreover, the addition rate of the acid or of the antisolvent has an influence on the size of the nanoparticles, with larger dimensions obtained with relatively fast mixing processes.[14]

Despite the relevant amount of experimental data concerning the preparation of nanoparticles through the modulation of the above-mentioned parameters, few reports explain these results on the basis of the supramolecular interactions driving the formation of LNPs.[28–30]

In this work, we aim to correlate the colloidal properties of softwood kraft lignin nanoparticles prepared using the solvent–antisolvent method to (i) the initial concentration of lignin, (ii) the different solvent : antisolvent systems, (iii) the rate of addition of the solvent and of the antisolvent, and (iv) the order of the addition of the antisolvent/solvent.

We therefore performed experiments using DMSO, acetone, ethylene glycol and THF as solvents and water as the antisolvent that were integrated with classical molecular dynamics simulations, in order to quantify the contribution of the different supramolecular interactions to the formation of the LNPs, with a focus on the resulting size and zeta potential.

2 Results and discussion

2.1 Effect of initial lignin concentration

The pristine softwood kraft lignin at different initial concentrations (Table S1†) was dissolved in DMSO and suspended in acetone (62% soluble fraction), ethylene glycol (30% soluble fraction) and THF (90% soluble fraction). The resulting soluble fractions were used to prepare LNPs *via* the solvent–antisolvent method (as described in Section 3.2).

It is important to underline that the mixtures of lignin in DMSO, ethylene glycol and THF used for the preparation of LNPs were solutions, not containing LNPs, as confirmed by DLS measurements.

Differently, when acetone was used to solubilize SKL, the presence of 230 nm LNPs was revealed *via* DLS measurements in the corresponding acetone-soluble fraction at a 6.6 mg mL^{-1} concentration. Therefore, this colloidal suspension was sequentially concentrated *via* rotary evaporation with the aim of investigating the effect of lignin concentration on the LNPs' size.

A complex trend was registered (Table 1): the initially larger LNPs (230 nm) underwent a decrease in their size by 26% (to 170 nm) at 40 mg mL^{-1}, while an increase to 267 nm was registered at 500 mg mL^{-1}. The initial LNP shrinkage following acetone removal could be ascribed to the increasingly likely lignin–lignin intrachain interactions (hydrogen bonds and π–π stacking), which induced the exclusion of acetone and yielded a lower hydrodynamic volume. The subsequent LNP enlargement could be related to the self-reorganization of lignin chains at a relatively low mass fraction of acetone (61% at 500 mg mL^{-1} *vs.* 99.9% at 6.6 mg mL^{-1}), where a significant fraction of the volume of the colloidal dispersion is occupied by lignin chains. Under these significantly modified

Table 1 LNPs' hydrodynamic diameters as function of the initial concentration of lignin in acetone. PDI: polydispersity index

Initial ASKL concentration/mg mL^{-1}	LNPs' hydrodynamic diameter/nm	PDI
6.6	230	0.04
17	198	0.28
40	170	0.22
500	267	0.28
1000	254	0.50

conditions, the interchain lignin interactions are expected to be dominant and contribute to the formation of larger LNPs.

As expected for the remaining lignin solutions, the addition of water as antisolvent induced the formation of LNPs with size ranging from 28 to 267 nm using DMSO as solvent, and from 24 to 768 nm using ethylene glycol, while 75–769 nm LNPs were obtained from THF (Table S1†), varying the addition rate and the order of addition (*i.e.*, solvent added into the antisolvent or *vice versa*).

DLS data revealed a general trend for LNPs prepared from DMSO and ethylene glycol, whose size increased when increasing the initial concentration of lignin (Fig. 1a). This trend was maintained independently from the addition rate and the order of addition. This behaviour generally indicates that the growth rate is faster than the nucleation rate during the nucleation and growth process (minimum supersaturation regime):[26,31] the aggregation number (*i.e.*, the average number of lignin chains per nanoparticle) becomes therefore higher, revealing a dominant contribution in terms of interchain hydrogen bonds and π–π interactions and resulting in larger LNPs.

An opposite trend was observed for controlled and non-controlled additions of THF lignin solution to H_2O, suggesting a maximum supersaturation regime, where the nucleation rate is faster than the growth rate, resulting in smaller LNPs. In this case, lignin intrachain interactions are anticipated to play a major role.

2.2 Effect of the rate of the addition of the solvent/antisolvent and of the order of addition

It was observed that the non-controlled (*i.e.*, extremely fast) addition of H_2O to DMSO lignin solutions (5 mg mL^{-1}) typically yielded LNPs with a lower hydrodynamic radius (37 nm) with respect to ethylene glycol (46 nm) and THF (310 nm), the latter presenting the largest LNP size (Fig. 1b). This trend was maintained also when inverting the addition sequence, *i.e.*, adding the organic solvent to water (DMSO, 32 nm; ethylene glycol, 52 nm; THF, 170 nm).

The order of addition was found to significantly influence the LNP size for the highest initial lignin concentrations in ethylene glycol : H_2O system (50 mg mL^{-1}): 768 nm LNPs were obtained adding ethylene glycol to water in a non-controlled way, while the reverse addition yielded 288 nm LNPs. An opposite trend was registered for the non-controlled addition in THF : H_2O system: 310 nm LNPs were obtained adding H_2O to THF, while the reverse addition resulted in 170 nm LNPs, using a 5 mg mL^{-1} initial lignin concentration.

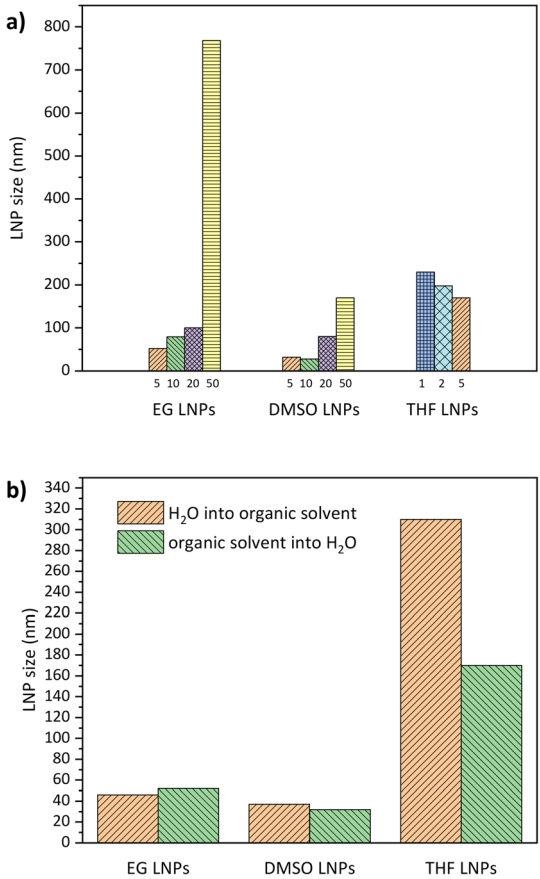

Fig. 1 (a) Variation of the LNPs' size as a function of the initial concentration of lignin (1, 2, 5, 10, 20 and 50 mg mL^{-1}). Data is from the non-controlled (*i.e.*, extremely fast) addition of the lignin solution into water. EG: ethylene glycol. (b) Variation of the LNPs' size as a function of the order of the addition. Non-controlled-addition data are reported (5 mg mL^{-1} initial lignin concentration).

The LNP size variations could not be correlated with the Flory–Huggins interaction parameters (χ_{PS})[32] of these three solvents at room temperature (0.7 for DMSO, 2.9 for THF and 5.1 for ethylene glycol), since THF would be expected to yield smaller LNPs with respect to ethylene glycol due to its greater stabilization of lignin chains, which prevents agglomeration/aggregation phenomena.

It is therefore reasonable to infer that kinetics play a major role in determining the size of LNPs. In order to investigate this aspect, the controlled addition of the antisolvent was performed using a peristaltic pump.

For the ethylene glycol : H_2O system, the controlled addition of ethylene glycol solutions into H_2O generally yielded stable LNPs with much smaller diameters than the ones obtained *via* a non-controlled addition, especially in the case of high lignin concentrations (*e.g.*, using 20 mg mL^{-1} lignin, 37 nm LNPs were obtained with 0.5 mL min^{-1} ethylene glycol addition *vs.* 108 nm LNPs obtained with non-controlled addition) (Table S1†).

For the system THF : H_2O, the controlled addition of lignin solutions to H_2O induced the formation of smaller LNPs with respect to non-controlled-addition experiments. Moreover, the controlled addition of H_2O to THF lignin solutions yielded the formation of larger LNPs with respect to the case of the non-controlled addition.

In the case of the system DMSO : H_2O, the controlled addition of lignin solutions into H_2O did not influence the size of the obtained LNPs (Table S1†).

Altogether, the effects of the addition rate of the organic solvent into H_2O on the LNPs' size could be attributed to conformational rearrangements of lignin chains necessary to form the first lignin nuclei, which subsequently evolve into LNPs. These conformational rearrangements occur with relatively slow kinetics with respect to the kinetics of interaction with H_2O molecules, as demonstrated by Jahan *et al.*[12] In this work, the lifetime of lignin–lignin hydrogen bonds was observed to increase as the H_2O molar fraction increased. This implies that a higher water content reduces the conformational freedom of lignin chains, preventing lignin inter- and intrachain hydrogen bonds from breaking for the conformational change to occur.

The experimental observations can therefore be explained as follows. The slow addition of the organic solvent into water causes a slow increase of lignin concentration in the final mixture. This favours the formation of nuclei with low aggregation numbers, minimizing the hydrodynamic volume of the final LNPs. On the other hand, a quick addition of the organic solvent creates spatially and temporally higher lignin concentrations, yielding nuclei with high aggregation numbers, which exhibit a larger hydrodynamic volume.

The experiments with DMSO : H_2O represent an exception, since the solvent addition rate did not have any influence on the size of the LNPs. It can be therefore inferred that the strong interactions between lignin and DMSO allowed the latter to maintain a certain degree of solvation around lignin chains. This would allow lignin conformational rearrangements to occur with relatively fast kinetics, even in the presence of a high molar fraction of water, to form nuclei with low aggregation numbers. This peculiar solvation state would also explain the fact that neither was the order of addition found to influence the final LNP hydrodynamic diameter.

2.3 Effect of lignin structure on LNPs' zeta potential

The LNPs prepared by adding the lignin DMSO solution into water were more colloidally stable than the ones obtained when reversing the order of addition (-56 mV for DMSO into H_2O *vs.* -21 mV for H_2O into DMSO at a 5 mg mL^{-1} initial lignin concentration; non-controlled addition) (Table S1†). For the case of the addition of DMSO into water, the colloidal stability was observed to decrease when increasing the initial concentration of lignin. Reversing the addition order resulted in an opposite trend. Conversely, more stable LNPs were formed by increasing the initial concentration of lignin using ethylene glycol, independently from the order of addition (Table S1†).

HSQC and ^{31}P-NMR spectra were obtained in order to investigate the structural differences between the pristine SKL lignin and the fractions that constitute the LNPs, and correlate these data with their zeta-potential values.

For these investigations, DMSO and ethylene glycol were selected as extremes in terms of the ability to solubilize lignin: DMSO yielded a complete

Table 2 Aliphatic, phenolic and carboxylic OH content of pristine SKL, SKL constituting LNPs prepared from DMSO (DMSO LNPs), and SKL constituting LNPs prepared from ethylene glycol (EG LNPs) as determined by ^{31}P-NMR. Values are expressed in mmol g^{-1}

		SKL	DMSO LNPs	EG LNPs
Aliphatic OH		1.90	0.93	1.12
Phenolic OH	Condensed OH	0.28	0.23	0.25
	Guaiacyl OH	1.21	0.84	1.02
	p-Hydroxyphenyl OH	0.01	0.02	0.01
	Total phenolic OH	1.50	1.09	1.28
Carboxylic OH		0.28	0.28	0.24

solubilization, while ethylene glycol exhibited the lowest soluble fraction (30%). Moreover, the non-controlled addition of water into the lignin solutions was chosen as the LNP preparation method.

HSQC spectra revealed that LNPs prepared from both DMSO and ethylene glycol under the above-mentioned experimental conditions presented a higher concentration of guaiacyl units (Table S2†), with respect to pristine SKL, suggesting the less condensed nature of the former.

^{31}P-NMR spectra registered a 51% decrease in aliphatic OH for LNPs prepared using the DMSO : H_2O system with respect to pristine SKL (Table 2). A similar behaviour was observed for ethylene glycol : H_2O LNPs (−41%). Concurrently, a decrease in the concentration of total phenolic OH was observed for both types of LNPs (27% for DMSO : H_2O, 14% for ethylene glycol : H_2O). The strongest contribution to this decrease was due to guaiacyl OH (−30% for DMSO : H_2O and −15% for ethylene glycol : H_2O) and to condensed OH (−18% for DMSO : H_2O and −11% for ethylene glycol : H_2O).

Altogether, the lignin fractions involved in the formation of the LNPs were generally less hydrophilic with respect to the pristine SKL, confirming previous evidence about the formation of a higher molecular weight core during the nucleation phase.[33]

The concentration of carboxyl groups in lignin constituting DMSO : H_2O LNPs was 17% higher than that registered for ethylene glycol : H_2O LNPs (0.28 *vs.* 0.24 mmol g^{-1}, respectively). Under neutral pH conditions, the condensed phenolic OH groups are deprotonated as well, presenting typical pK_a values ranging from 6 to 7.[34] In this case, DMSO : H_2O LNPs presented non-significantly different values with respect to ethylene glycol : H_2O ones (0.23 *vs.* 0.25 mmol g^{-1}, respectively). Overall, the concentration of deprotonated functional groups (carboxyl + condensed OH) were non-significantly different between DMSO : H_2O LNPs (0.51 mmol g^{-1}) and ethylene : glycol ones (0.49 mmol g^{-1}).

The more stable zeta potential of LNPs prepared using DMSO as solvent with respect to ethylene glycol : H_2O ones (Table S1†) could not therefore be attributed to differences in the total concentration of deprotonatable functional groups. The major contribution was attributed to the size difference: the LNPs synthesised using DMSO were generally smaller with respect to the ones prepared using ethylene glycol (Table S1†), the higher surface-area-to-volume ratio of the former causing a higher concentration of OH groups to be exposed on the surface of the LNPs.

2.4 Supramolecular interactions in LNPs prepared using the solvent–antisolvent method

To better understand the nature of the supramolecular interactions that define lignin behaviour in the preparation of LNPs using the solvent–antisolvent method, classical molecular dynamics (MD) simulations of lignin in DMSO and in ethylene glycol in the presence of different water concentrations were performed. The structures of acetone-soluble (ASKL, 4 structures) and acetone-insoluble (AIKL, 1 structure) fractions proposed by Crestini *et al.*[10] were used as initial structures for the MD simulations (Fig. S1†).

Compared to the globular shape adopted by AIKL in a vacuum, where intramolecular hydrogen bonds and π–π stacking interactions are dominant (Fig. 2a), an extended conformation was obtained in pure DMSO (see Fig. 2b), which is known to dissolve lignin without fractionating it.[32,35] This was ascribed to the ability of DMSO to interact both with polar and non-polar regions of lignin chains, disrupting lignin intrachain hydrogen bonds but not inducing hydrophobic collapse. On the other hand, ethylene glycol, which is not able to fully solubilize lignin[36] and is endowed with polar OH groups and a weakly non-polar ethyl chain,

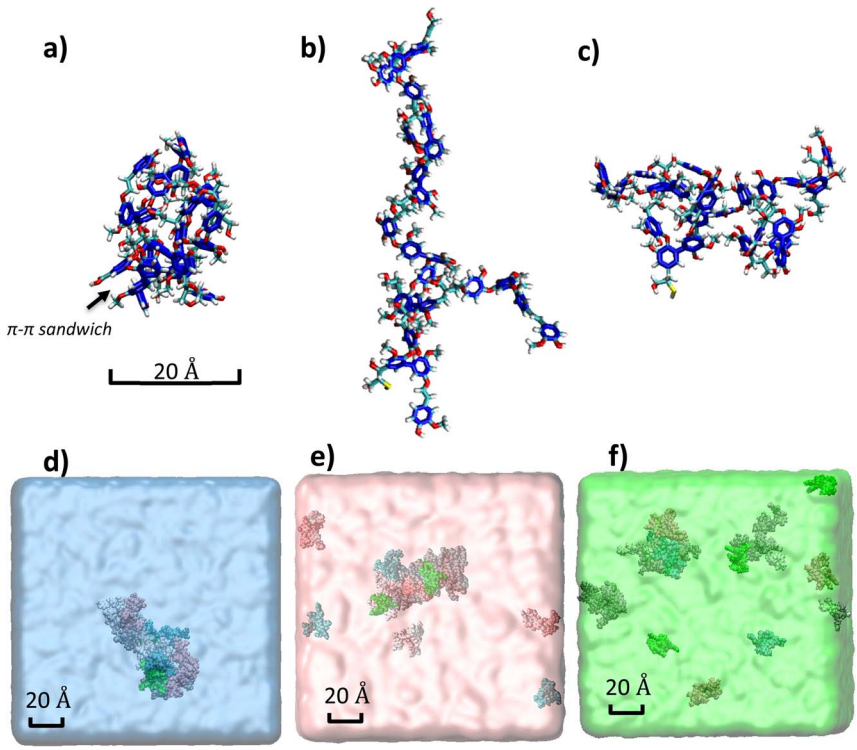

Fig. 2 Representative snapshots from classical molecular dynamics simulations. AIKL molecule (a) in a vacuum, (b) in DMSO and (c) in ethylene glycol (colours: dark blue – aromatic rings of AIKL; for atoms: cyan – C, red – O, white – H, yellow – S). (d–f) Largest lignin nuclei observed in (d) pure water, (e) DMSO with 60% water, and (f) ethylene glycol with 60% water (colours: grey – AIKL, green – ASKL-A; white – ASKL-B; pink – ASKL-C; cyan – ASKL-D) (for the corresponding structures, see Fig. S1†).

induced a hydrophobic collapse of the AIKL structure. The resulting globular conformation was less compact with respect to the one calculated in a vacuum (Fig. 2c), indicating that the lignin intramolecular interactions are weaker compared to the ones exhibited in a vacuum.

The variations in the average number of intramolecular hydrogen bonds and π–π interactions for a single AIKL molecule in different environments clearly demonstrate the influence of the solvent on the molecular conformation and physical interactions. In the MD simulations, the average number of intramolecular hydrogen bonds was 8 for the globular conformation of AIKL in a vacuum, 2 for the extended conformation in DMSO, and 5 in ethylene glycol.

The total number of π–π stacking interactions showed a less pronounced variation in the different environments. Nevertheless, a more detailed analysis distinguishing between sandwich and T-shaped stacking types revealed a notable trend: a decrease in sandwich-type stacks and a corresponding increase in T-shaped interactions. Specifically, the average number of sandwich-type stacks (with the total number of π–π interactions in parentheses) was: 4 (11) in vacuum, 3 (10) in ethylene glycol, and 2 (10) in DMSO.

Since sandwich-type interactions are approximately twice as energetically favourable as the T-shaped ones, this shift in their number may contribute to the observed differences in structural stability and compactness.

The reduction in intramolecular hydrogen bonding was accompanied by an increase in hydrogen bonding between AIKL and solvent molecules: on average, 18 hydrogen bonds were formed with DMSO and 32 with ethylene glycol. This difference could be attributed to the hydrogen-bonding capacity of the solvents: DMSO acts only as a hydrogen bond acceptor, whereas ethylene glycol functions as both a donor and acceptor.

The standard error for all reported values is less than 1.

We can therefore propose that, in the solubilization step, lignin intrachain hydrogen bonds are cleaved and stronger lignin–solvent hydrogen bonds are formed, resulting in a higher hydrodynamic volume occupied by the lignin chains. Moreover, the solubilization is accompanied by a reduction of sandwich π–π stackings and by an increase in the T-shaped ones, further corroborating the increase in the hydrodynamic volume of the lignin nuclei.

In order to study the formation of the first lignin nuclei induced by the addition of water, a simulation unit cell containing 3 sets of lignin structures, *i.e.*, 3 AIKL + 12 ASKL structures, was used. These lignin structures were initially optimized in a vacuum and subsequently equilibrated in DMSO, as described in Section 3.6.

Very weak interactions between lignin chains were obtained in pure DMSO, as reflected by the number of inter- and intramolecular hydrogen bonds (10) and π–π stackings (4) of the sandwich type for the whole system containing 15 lignin molecules in the simulation cell (Table S3†).

An increasing percentage of water (20%, 40% and 60%) in the DMSO system induced the clusterization of lignin chains (Fig. 2e): the non-stable and loosely bound nuclei observed at 20% water content evolved into larger and more stable ones at 60% water content. The fastest clusterization kinetics were found for the highest water content. Moreover, at 60% water content, 10 lignin chains clustered to form one single nucleus, while in the case of lower water content, the nuclei showed lower aggregation numbers. Therefore, MD simulations (Table S3†)

proved that the water-induced nucleation process causes a significant increase in π–π stacking interactions between lignin chains.

A similar behaviour was observed upon addition of water to the ethylene glycol system, but with a less marked clusterization trend (Fig. 2f). This effect could be ascribed to the hydrophobically collapsed globular conformation of lignin chains in ethylene glycol, which prevents the formation of π–π stackings between the buried regions of different lignin chains.

The maximum degree of clusterization was reached in pure water, where one single cluster consisting of 15 lignin chains was formed (Fig. 2d).

In light of these data, we can propose that, in the antisolvent addition step, interchain lignin hydrogen bonds and π–π stacking interactions were established (Table S3†). Concurrently, lignin chains formed nuclei where the hydrophobic moieties clustered together, while the hydrophilic OH groups interacted with water molecules.

Altogether, the classical MD simulations were able to elucidate the underlying driving forces involved in the creation of the first SKL lignin nuclei, formed on a submicrosecond timescale, using the solvent–antisolvent method.

3 Methods

3.1 Materials

Softwood kraft lignin (SKL) was provided by Stora Enso. DMSO, ethylene glycol, THF, acetone, pyridine (anhydrous, 99.8%), chromium acetylacetonate (99.99%), 2-chloro-4,4,5,5-tetramethyl-1,3,2-dioxaphospholane (Cl-TMDP, 95%), *N*-hydroxy-5-norbornene-2,3-dicarboxylic acid imide (NHND, 97%), DMSO-d_6 and $CDCl_3$ were purchased from Sigma-Aldrich. Ultrapure water produced by means of a Milli-Q® Reference system that generates type I ultrapure water (18.2 MΩ cm resistivity @25 °C, ≤5 ppb total organic carbon (TOC)) was used in the experiments.

3.2 Synthesis of LNPs *via* the solvent–antisolvent method

The LNPs were synthesized according to the following procedure. First, the appropriate amount of SKL was dispersed in 70 mL of the corresponding analytical grade organic solvent (DMSO, ethylene glycol and THF; see Table S1† for the corresponding initial lignin concentrations). The resulting dispersions were kept stirring for 24 hours. Subsequently, the dispersions were centrifuged (23 269*g*, 10 min, 20 °C) to separate any undissolved residuals (DMSO: no residuals; acetone: 38% wt residuals; ethylene glycol: 70% wt residuals; THF: 10% wt residuals). The supernatant was kept stirring at 1500 rpm and was diluted by adding 630 mL of distilled water (DMSO/ethylene glycol/THF : water ratio = 1 : 10). The rates of addition for the preparation of LNPs are indicated in Table S1.† The controlled-addition experiments were conducted using a peristaltic pump (Legato 200, KD Scientific). The obtained dispersion was centrifuged (23 269*g*, 25 min, 20 °C) to recover the LNPs, which were subsequently freeze-dried. LNP yields: DMSO, 158.3 mg (11.3%); ethylene glycol, 68.4 mg (4.9%); THF 140.1 mg (10%).

3.3 Characterization of LNPs

Dynamic light scattering (DLS) analyses of the LNPs were carried out by means of a Malvern Zetasizer Ultra instrument to assess the LNPs' size (1–1000 nm) and zeta potential. A folded capillary zeta cell (DTS1070, Malvern Panalytical) was employed for zeta-potential measurements.

3.4 Quantitative ^{31}P-NMR analyses

Quantitative ^{31}P-NMR analysis was performed as previously reported.[37,38] In brief, accurately weighed amounts of pristine SKL (18.2 mg), LNPs prepared using the DMSO : H_2O system (26.1 mg) and LNPs prepared using the ethylene glycol : H_2O system (14.3 mg) were phosphorylated using 2-chloro-4,4,5,5-tetramethyl-1,3,2-dioxaphospholane (Cl-TMDP) and the spectra were recorded on a Bruker 300 MHz spectrophotometer (128 scans at 20 °C, relaxation delay 12 s). *N*-Hydroxy-5-norbornene-2,3-dicarboxylic acid imide (NHND) was used as an internal standard, and chromium(III) acetylacetonate as a relaxation agent. All chemical shifts reported are relative to the reaction product of water with Cl-TMDP, which gives a sharp signal in pyridine/$CDCl_3$ at 132.2 ppm.

3.5 HSQC analyses

Solutions of SKL (337 mg mL^{-1}), LNPs prepared using the DMSO : H_2O system (264 mg mL^{-1}) and LNPs prepared using the ethylene glycol : H_2O system (171 mg mL^{-1}) were prepared in a 1 : 1 pyridine-d_5 : DMSO-d_6 mixture. The corresponding HSQC spectra were recorded on a Bruker 400 MHz NMR (32 scans) with an acquisition delay of 0.256 s and a relaxation delay of 2 s.

3.6 MD simulations

Single molecules of water, dimethyl sulfoxide (DMSO) and ethylene glycol were built and optimised using Avogadro.[39] The parametrisation of lignin chains and solvent molecules was performed *via* well-established protocols for nonpolarizable CHARMM[40] force fields using CGenFF.[41,42]

To assess the direct influence of solvents, the initial configurations of lignin molecules were first simulated in a vacuum for 20 ns. Following this step, the resulting structures were individually solvated in cubic boxes ($50 \times 50 \times 50$ Å^3) containing either ethylene glycol or DMSO. After equilibration, these solvated lignin structures were extracted and randomly placed into larger systems containing 15 lignin molecules (3 molecules of each chain type; see Fig. S1†) using Packmol 20.010 (tolerance = 2 Å).[43]

The number of solvent molecules in each system—with variation of water concentrations—was calculated based on standard relationships among density, molar concentration, and relative concentration.

The final simulation boxes for nanoparticle formation with 15 lignin molecules measured $150 \times 150 \times 150$ Å^3.

The simulations of single lignin molecules and LNPs in solvents were conducted in two stages with periodic boundary conditions in all three spatial directions. Each system was initially equilibrated for 20 ns, and a further productive run was performed for 180 ns. For both stages, the NPT ensemble in NAMD 2.12 was used.[44] The pressure was maintained at 1 atm using the Langevin

piston method, while the temperature was controlled at 298 K with a Langevin thermostat (damping coefficient of 1 ps^{-1}). The SETTLE algorithm was employed to constrain bonds involving hydrogen atoms, allowing a 2 fs integration timestep. Short-range nonbonded interactions were computed using a 12 Å cutoff. Long-range electrostatics were treated with the particle mesh Ewald (PME) method using a grid spacing of 1.0 Å. The production trajectories were subsequently analysed using VMD 1.9.3 (ref. 45) to quantify changes in the number of hydrogen bonds (tool Hydrogen Bonds) and π–π stacking interactions (tcl script; see ESI†).

The average numbers of hydrogen bonds and π–π stacks of lignin in solvents were calculated for the last 50 ns of the productive run. The parameters for hydrogen-bond counting were: donor–acceptor distance 3.2 Å, angle cutoff 30°.

4 Conclusions

In summary, we prepared lignin nanoparticles from softwood kraft lignin using different solvent–antisolvent systems, where water was used as the antisolvent.

The size of the final LNPs was found to increase when increasing the initial concentration of lignin for DMSO and ethylene glycol (minimum supersaturation regime), while the opposite trend was observed for THF (maximum supersaturation regime).

Kinetic effects concerning the conformational rearrangements of lignin chains were found to influence the size of LNPs: the slow addition of THF and ethylene glycol solutions into water caused the formation of nuclei with low aggregation numbers, minimizing the hydrodynamic volume of the final LNPs. On the other hand, a quick addition of these lignin solutions yielded nuclei with high aggregation numbers, exhibiting a larger hydrodynamic volume.

The zeta potential of LNPs was found to be mainly determined by the superficial concentration of carboxylic acid and condensed guaiacyl units, which was assessed to be higher for the smaller DMSO LNPs, thanks to the higher surface-area-to-volume ratio.

Classical molecular dynamics simulations were performed to understand the driving forces responsible for the formation of the first lignin nuclei after water addition. The calculations revealed that the interchain lignin hydrogen bonds and π–π stacking interactions induce the formation of lignin nuclei, where the hydrophobic moieties cluster together, while the hydrophilic OH groups interact with water molecules.

Altogether, these results contribute to expanding the knowledge about the supramolecular interactions driving the nucleation of lignin nanoparticles, with a view to the full exploitation of lignin as a key material for sustainable technological applications.

Abbreviations

AIKL	Acetone-insoluble kraft lignin
ASKL	Acetone-soluble kraft lignin
CGenFF	CHARMM general force field
CHARMM	Chemistry at HARvard macromolecular mechanics

Cl-TMDP	2-Chloro-4,4,5,5-tetramethyl-1,3,2-dioxaphospholane
DLS	Dynamic light scattering
DLVO	Derjaguin, Landau, Verwey, and Overbeek
DMSO	Dimethyl sulfoxide
EG	Ethylene glycol
HSQC	Heteronuclear single quantum coherence spectroscopy
LNPs	Lignin nanoparticles
MD	Molecular dynamics
NAMD	NAnoscale molecular dynamics
NHND	*N*-Hydroxy-5-norbornene-2,3-dicarboxylic acid imide
PME	Particle mesh Ewald
SKL	Softwood kraft lignin
THF	Tetrahydrofuran
TOC	Total organic carbon
VMD	Visual molecular dynamics

Data availability

The data supporting this article have been included as part of the ESI.†

Conflicts of interest

There are no conflicts to declare.

Acknowledgements

This study was carried out within the projects "ENhanced CAtalytic fractionation and depolymerization Processes for a Straightforward valorization of lignocellU-Losic biomass to chemicals and mATErials (ENCAPSULATE)" and "Thorough Upcycling of Rice waste biomass into BiOactive PACKaging *via* chemoenzymatic processes (TURBOPACK)" and received funding from the European Union Next-GenerationEU – National Recovery and Resilience Plan (NRRP) – MISSION 4 COMPONENT 2, INVESTIMENT 1.1 Fondo per il Programma Nazionale di Ricerca e Progetti di Rilevante Interesse Nazionale (PRIN) – CUP N. H53D23003890001 (ENCAPSULATE) and H53D23007900001 (TURBOPACK), respectively. This manuscript reflects only the authors' views and opinions; neither the European Union nor the European Commission can be considered responsible for them.

Notes and references

1 C. Libretti, L. S. Correa and M. A. R. Meier, *Green Chem.*, 2024, **26**, 4358–4386.
2 K. Li, W. Zhong, P. Li, J. Ren, K. Jiang and W. Wu, *Int. J. Biol. Macromol.*, 2023, **251**, 125992.
3 K. Li, W. Zhong, P. Li, J. Ren, K. Jiang and W. Wu, *Int. J. Biol. Macromol.*, 2023, **252**, 126281.
4 X. Wu, H. Lian, C. Xia, J. Deng, X. Li and C. Zhang, *Int. J. Biol. Macromol.*, 2024, **280**, 135477.

5 L. Dessbesell, M. Paleologou, M. Leitch, R. Pulkki and C. Charles) Xu, *Renewable Sustainable Energy Rev.*, 2020, **123**, 109768.
6 C. Crestini, F. Melone, M. Sette and R. Saladino, *Biomacromolecules*, 2011, **12**, 3928–3935.
7 J. Ralph, K. Lundquist, G. Brunow, F. Lu, H. Kim, P. F. Schatz, J. M. Marita, R. D. Hatfield, S. A. Ralph, J. H. Christensen and W. Boerjan, *Phytochem. Rev.*, 2004, **3**, 29–60.
8 H. Lange, S. Decina and C. Crestini, *Eur. Polym. J.*, 2013, **49**, 1151–1173.
9 P. Sannigrahi, Y. Pu and A. Ragauskas, *Curr. Opin. Environ. Sustain.*, 2010, **2**, 383–393.
10 C. Crestini, H. Lange, M. Sette and D. S. Argyropoulos, *Green Chem.*, 2017, **19**, 4104–4121.
11 E. Melro, L. Alves, F. E. Antunes and B. Medronho, *J. Mol. Liq.*, 2018, **265**, 578–584.
12 N. Jahan, M. M. Huda, Q. X. Tran and N. Rai, *J. Phys. Chem. B*, 2022, **126**, 5752–5764.
13 R. Li, D. Huang, S. Chen, L. Lei, Y. Chen, J. Tao, W. Zhou and G. Wang, *Nanoscale*, 2022, **14**, 10299–10320.
14 R. Trovagunta, R. Marquez, L. Tolosa, N. Barrios, F. Zambrano, A. Suarez, L. Pal, R. Gonzalez and M. A. Hubbe, *Adv. Colloid Interface Sci.*, 2024, **332**, 103247.
15 N. Pajer, C. Cestari, D. S. Argyropoulos and C. Crestini, *npj Mater. Sustain.*, 2024, **2**, 1–9.
16 M. Gigli, G. Fellet, L. Pilotto, M. Sgarzi, L. Marchiol and C. Crestini, *Front. Plant Sci.*, 2022, **13**, 976410.
17 B. Abraham, V. L. Syamnath, K. B. Arun, P. M. Fathima Zahra, P. Anjusha, A. Kothakotta, Y.-H. Chen, V. K. Ponnusamy and P. Nisha, *Sci. Total Environ.*, 2023, **881**, 163316.
18 B. Du, W. Li, Y. Bai, Z. Pan, Q. Wang, X. Wang, H. Ding, G. Lv and J. Zhou, *Int. J. Biol. Macromol.*, 2022, **214**, 170–180.
19 M. Witzler, A. Alzagameem, M. Bergs, B. E. Khaldi-Hansen, S. E. Klein, D. Hielscher, B. Kamm, J. Kreyenschmidt, E. Tobiasch and M. Schulze, *Molecules*, 2018, **23**, 1885.
20 M. H. Hussin, J. N. Appaturi, N. E. Poh, N. H. A. Latif, N. Brosse, I. Ziegler-Devin, H. Vahabi, F. A. Syamani, W. Fatriasari, N. N. Solihat, A. Karimah, A. H. Iswanto, S. H. Sekeri and M. N. M. Ibrahim, *Int. J. Biol. Macromol.*, 2022, **200**, 303–326.
21 I. V. Pylypchuk, A. Riazanova, M. E. Lindström and O. Sevastyanova, *Green Chem.*, 2021, **23**, 3061–3072.
22 L. Chen, S.-M. Luo, C.-M. Huo, Y.-F. Shi, J. Feng, J.-Y. Zhu, W. Xue and X. Qiu, *Green Chem.*, 2022, **24**, 285–294.
23 Y. Bai, X. Wang, X. Wang, X. Yang, X. Li, H. Xin, D. Sun and J. Zhou, *Front. Chem.*, 2022, **10**, 1107643.
24 M. Gigli, S. Cailotto and C. Crestini, in *Biorefinery: from Biomass to Chemicals and Fuels*, De Gruyter, 2021, pp. 265–320.
25 C. Frangville, M. Rutkevičius, A. P. Richter, O. D. Velev, S. D. Stoyanov and V. N. Paunov, *ChemPhysChem*, 2012, **13**, 4235–4243.
26 A. Manisekaran, P. Grysan, B. Duez, D. F. Schmidt, D. Lenoble and J.-S. Thomann, *J. Colloid Interface Sci.*, 2022, **626**, 178–192.

27 E. Lizundia, M. H. Sipponen, L. G. Greca, M. Balakshin, B. L. Tardy, O. J. Rojas and D. Puglia, *Green Chem.*, 2021, **23**, 6698–6760.
28 J. Wang, W. Chen, D. Yang, Z. Fang, W. Liu, T. Xiang and X. Qiu, *Small*, 2022, **18**, 2200671.
29 R. C. Andeme Ela, S. Raza, P. A. Heiden, J. V. Vermaas and R. G. Ong, *ACS Appl. Polym. Mater.*, 2022, **4**, 6925–6935.
30 L. Chen, S.-M. Luo, C.-M. Huo, Y.-F. Shi, J. Feng, J.-Y. Zhu, W. Xue and X. Qiu, *Green Chem.*, 2022, **24**, 285–294.
31 M. Çelikbilek Ersundu, A. E. Ersundu and S. Aydin, in *Advances in Crystallization Processes*, ed. Y. Mastai, IntechOpen, Rijeka, 2012.
32 V. Passoni, C. Scarica, M. Levi, S. Turri and G. Griffini, *ACS Sustain. Chem. Eng.*, 2016, **4**, 2232–2242.
33 M. H. Sipponen, H. Lange, M. Ago and C. Crestini, *ACS Sustain. Chem. Eng.*, 2018, **6**, 9342–9351.
34 M. Ragnar, C. T. Lindgren, N.-O. Nilvebrant and J. Wood, *Chem. Technol.*, 2000, **20**, 277–305.
35 A. Duval, F. Vilaplana, C. Crestini and M. Lawoko, *Holzforschung*, 2016, **70**, 11–20.
36 L. Mu, Y. Shi, H. Wang and J. Zhu, *ACS Sustain. Chem. Eng.*, 2016, **4**, 1840–1849.
37 X. Meng, C. Crestini, H. Ben, N. Hao, Y. Pu, A. J. Ragauskas and D. S. Argyropoulos, *Nat. Protoc.*, 2019, **14**, 2627–2647.
38 D. S. Argyropoulos, N. Pajer and C. Crestini, *J. Vis. Exp.*, 2021, e62696.
39 M. D. Hanwell, D. E. Curtis, D. C. Lonie, T. Vandermeersch, E. Zurek and G. R. Hutchison, *J. Cheminf.*, 2012, **4**, 17.
40 J. V. Vermaas, L. Petridis, J. Ralph, M. F. Crowley and G. T. Beckham, *Green Chem.*, 2019, **21**, 109–122.
41 K. Vanommeslaeghe and A. D. Jr. MacKerell, *J. Chem. Inf. Model.*, 2012, **52**, 3144–3154.
42 K. Vanommeslaeghe, E. Hatcher, C. Acharya, S. Kundu, S. Zhong, J. Shim, E. Darian, O. Guvench, P. Lopes, I. Vorobyov and A. D. Mackerell Jr, *J. Comput. Chem.*, 2010, **31**, 671–690.
43 L. Martínez, R. Andrade, E. G. Birgin and J. M. Martínez, *J. Comput. Chem.*, 2009, **30**, 2157–2164.
44 J. C. Phillips, D. J. Hardy, J. D. C. Maia, J. E. Stone, J. V. Ribeiro, R. C. Bernardi, R. Buch, G. Fiorin, J. Hénin, W. Jiang, R. McGreevy, M. C. R. Melo, B. K. Radak, R. D. Skeel, A. Singharoy, Y. Wang, B. Roux, A. Aksimentiev, Z. Luthey-Schulten, L. V. Kalé, K. Schulten, C. Chipot and E. Tajkhorshid, *J. Chem. Phys.*, 2020, **153**, 044130.
45 W. Humphrey, A. Dalke and K. Schulten, *J. Mol. Graphics*, 1996, **14**, 33–38.